

# Influence of Different Defects on the Energy Bands for the Super Cell of a Defected Periodic Viaduct

Cheng-yong He<sup>#1</sup>, Li Lei<sup>#2</sup>

<sup>#</sup>Department of Civil Engineering and Mechanics, Jiangsu University, Zhenjiang 212013, China

**Abstract--** In this study, the influence of different defects on the energy bands for the super cell of a defected periodic viaduct (DPV) when considering the pile-soil-structure interaction is investigated. By developing a coupled boundary element method (BEM) model for the piles supporting the superstructure of the DPV, the compliances of the pile foundation can be obtained, combined with the transfer matrices for the beams and piers, the transfer matrix for each span of the viaduct can be determined. Then, the eigenvalue equation for the super cell of the DPV can be derived by utilizing the Bloch theorem, solution of which yields the energy bands of the super-cell. Numerical results show that some defects may give rise to the defect state for the super cell of the DPV.

**Keywords--** Defected periodic viaduct (DPV); super-cell method; the boundary element method (BEM); the pile-soil-structure interaction.

## I. INTRODUCTION

As viaduct can be used to resolve the settlement of soft soil bases effectively, they are now widely used in the high speed railways. For convenience, viaducts in normal sections are usually designed to consist of identical spans, so they can be simplified as periodic structures. For periodic viaducts with super long spans, they can be further idealized as infinite periodic structures. However, due to practical requirements, some spans of the viaduct are not identical with the standard span, making the viaduct defected. In this study, the spans different from the standard span are referred to as defected spans, and a periodic viaduct containing defected spans is called a defected periodic viaduct (DPV) [1-2].

Brillouin [3], Mead [4-6] and Lin [7] analyzed wave propagation in common periodic structures, and their researches show that waves in periodic structures are quite different from those in continuum media and the passband and stopband characteristics of the waves usually occurs in a periodic structure. It is noted that the behaviors of waves in a defected periodic structure is even more complicated than those in common periodic structures. By numerical simulation, Wu [8-9] found that in a defected periodic continuum medium, sharp peak occurs around the defected cell in a mode relevant to defected states. Up to now, there have been also some studies concerned with defected beams. Lin & Yang [10-11] analyzed a periodic beam with random defects, Mead [12-14] investigated the free waves propagating along a periodic beam with a single defect. Based on the researches of Mead, Bansal [15] investigated periodic structures with multiple defects and found that the influence of defects on the wave propagating along a periodic beam is significant because of

wave localization. Furthermore, Mead & Bansal [16] studied the response of a mono-coupled periodic beam with a single defect to a convected loading, finding that wave motion in the defected periodic beam may be confined around the defect. In summary, the presence of defected spans in a periodic beam may alter the characteristics of the wave motion, causing the localization of wave motion around the defects.

To investigate the defect state of the DPV, it is necessary to define a super-cell for the DPV. The super-cell of the viaduct should contain the defected span and also it should contain sufficient number of spans of the viaduct to make the responses of the super-cell associated with the defect state mode negligible at the edges of the super-cell. Since there has been no research addressing the influence of different defects on the energy bands for the super cell of a DPV so far, this paper will look into it. Besides, existing studies concerned about the beam-type periodic structure with defects are usually limited to continuous periodic beams, wherein beams are supposed to be continuous and supported by various periodically placed supporters. Since the viaduct considered in this study consists of a series of separate beams, piers and supporting piles, it is unreasonable to simplify the viaduct as a continuous beam.

## II. THE GENERAL STATEMENT AND APPROCH FOR THE PROBLEM IN THIS STUDY

Generally, a practical viaduct may be decomposed into two parts: substructure and superstructure. For simplicity, it is supposed in this study that each span of the viaduct only contains one pier and each pier of the viaduct is supported by an effective pile foundation. Also, the piers and piles are assumed to be rigidly connected. In this way, the substructure of the viaduct is simplified as a pile row embedded in the half-space soil as shown in Figure 1.

The superstructure of the periodic viaduct is reduced to a unit composed of a pier, two composite beams (left and right beams) and three linking springs, that is, the beam-beam, left and right beam-pier springs, respectively (Figure 1). The three springs form the beam-beam-pier (BBP) junction for each span of the viaduct.

It is supposed in this study that the periodic viaduct contain a defected span and the defected span is the 0-th span of the defected viaduct. Then,  $-\infty$  to  $-1$  spans and  $1$  to  $+\infty$  spans of the defected viaduct are the left and right semi-infinite periodic viaducts, respectively.

Generally, when a periodic viaduct is undergoing vibration, both the in-plane and out-of-plane vibrations may occur. Note that: the plane here is referred to as the plane passing through

the viaduct, namely, the  $xoz$  plane in Figure 1. Since the half-space soil, piles and super-structure of the viaduct in this study are assumed to be material and geometrically linear, the in-plane and out-of-plane vibrations of the viaduct are thus decoupled and the in-plane and out-of-plane vibrations of the viaduct can thus be investigated independently.

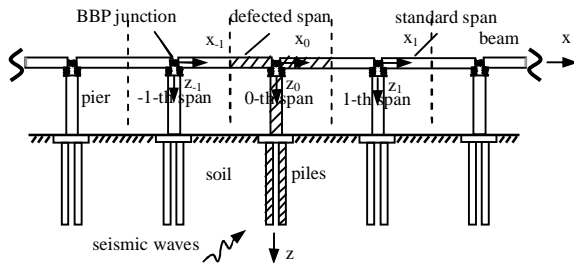


Fig. 1 Illustration for an infinite DPV

### III. A COUPLED BEM MODEL FOR THE PILE-SOIL INTERACTION PROBLEM

To account for the coupling between the superstructure of the viaduct and the pile foundations, the pile-soil interaction problem should be solved first. Since the separations between the neighboring effective piles are large enough, the interaction between them is neglected in this study, then, the multiple pile soil interaction problem is thus reduced to a single pile soil interaction problem. In this section, a coupled BEM model for a single pile embedded in the half-space soil will be developed, whereby the compliances of the pile foundation can be determined.

#### A. Boundary Integral Equation for an Elastic Medium

In this study, the pile and half-space soil are treated as the elastic medium. The equation of motion for an elastic medium in the frequency domain has the following expression [17]

$$\mu u_{i,jj} + (\lambda + \mu) u_{j,ji} = -\rho \omega^2 u_i \quad (1)$$

in which  $\lambda$  and  $\mu$  are the Lamé constants of the elastic medium;  $u_i$  is the displacement;  $\rho$  is the density;  $\omega$  is the angular frequency. Note that the frequency domain variable and time domain variable are related to each other by the Fourier transform for time and frequency. In this study, the Fourier transform with respect to time and frequency is defined as follows [18]

$$\hat{f}(\omega) = \int_{-\infty}^{+\infty} f(t) e^{-i\omega t} dt, \quad f(t) = \frac{1}{2\pi} \int_{-\infty}^{+\infty} \hat{f}(\omega) e^{i\omega t} d\omega \quad (2)$$

in which  $t$  represent the time, the variable with a caret denotes the frequency domain variable. Note that as this study is restricted to the frequency domain analysis of the defected viaduct, for brevity, the caret denoting the frequency domain variable is dropped for all the frequency domain variables. The constitutive relation for the elastic medium as follows [17]

$$\sigma_{ij} = 2\mu \varepsilon_{ij} + \lambda \delta_{ij} e \quad (3)$$

in which  $\sigma_{ij}$  and  $\varepsilon_{ij}$  are the stress and strain components for the elastic medium, respectively,  $e$  and  $\delta_{ij}$  denotes the bulk strain and the Kronecker delta, respectively. Based on the dynamic reciprocal theorem, the frequency domain boundary integral equation for the elastic medium is obtained as follows [19]

$$c_{ij} u_j(x) = \int_{\Gamma} [U_{ij}^{(G)}(\mathbf{x}, \mathbf{y}) t_j(y) - T_{ij}^{(G)}(\mathbf{x}, \mathbf{y}) u_j(y)] d\Gamma(y) \quad (4)$$

in which  $U_{ij}^{(G)}, T_{ij}^{(G)}$  are the Green's functions for the elastic medium and are given in Appendix A;  $u_j, t_j$  are the displacements and tractions along the boundary of the elastic medium;  $c_{ij}$  is the coefficients for the boundary and  $\Gamma$  denotes the boundary of the elastic medium.

#### B. Derivation of the Coupled BEM Model for the Pile and Half-Space Soil

In this section, according to the boundary integral equations for the elastic medium, boundary element formulations for the pile and half-space soil are established, respectively. By using the boundary element formulations as well as the boundary conditions and continuity conditions at the pile-soil interface, a coupled BEM model for the pile and half-space soil will be developed. As shown in Figure 2, for a pile embedded in a half-space soil, the whole boundary of the pile-soil system consists of three parts, that is, the interface between the pile and half-space soil ( $\Gamma_1$ ), the boundary of the pile top ( $\Gamma_2$ ), and the surface of the half-space soil ( $\Gamma_3$ ), respectively. The boundary of the pile consists of  $\Gamma_1$  and  $\Gamma_2$ , respectively and the boundary of the half-space soil is composed of  $\Gamma_1$  and  $\Gamma_3$ , respectively.

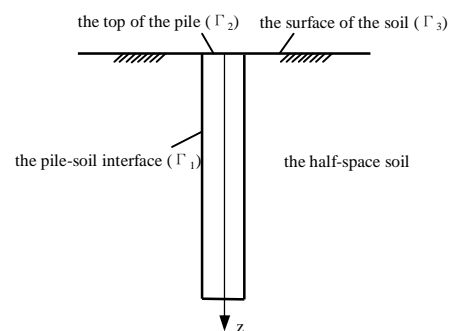


Fig. 2 The illustration for a pile embedded in an elastic half-space soil

The frequency domain integral equations for the pile and half-space soil can be discretized if suitable numbers of boundary elements are used to discretize the corresponding

boundaries. Suppose that the boundaries of the pile and half-space soil are discretized by the same type of iso-parametric element, each boundary element containing  $N_{nd}$  nodes. Thus, for a point  $\mathbf{x}$  inside the  $j$ -th element, the following interpolation formulae hold [20]

$$\mathbf{x}^{(j)}(\xi, \eta) = \sum_{n=1}^{N_{nd}} N_n(\xi, \eta) \mathbf{x}_n^{(j)}, \quad \mathbf{u}^{(j)}(\kappa, \mathbf{x}^{(j)}) = \sum_{n=1}^{N_{nd}} N_n(\xi, \eta) \mathbf{u}_n^{(j)}(\kappa),$$

$$\mathbf{t}^{(j)}(\kappa, \mathbf{x}^{(j)}) = \sum_{n=1}^{N_{nd}} N_n(\xi, \eta) \mathbf{t}_n^{(j)}(\kappa) \quad (5)$$

where the superscript  $j$  denotes the element number,  $n$  is the local node number,  $\xi, \eta$  are the intrinsic coordinates corresponding to the point  $\mathbf{x}^{(j)}$ ,  $\mathbf{x}_n^{(j)}$  is the  $n$ -th node coordinate of the  $j$ -th element in the global coordinate system,  $N_n(\xi, \eta)$  is the  $n$ -th shape function,  $\mathbf{u}_n^{(j)}(\kappa)$  and  $\mathbf{t}_n^{(j)}(\kappa)$  represent the displacement and traction vectors at the  $n$ -th node of the  $j$ -th element.

Using equation (5) in the boundary integral equation for the pile and integrating the shape function kernel products over all boundary elements for the pile, the boundary element formulation for the pile is obtained as follows

$$\mathbf{H}^{(p)} \mathbf{u}^{(p)} = \mathbf{G}^{(p)} \mathbf{t}^{(p)} \quad (6)$$

in which the superscript  $p$  denotes the pile;  $\mathbf{G}^{(p)}$  and  $\mathbf{H}^{(p)}$  are the coefficient matrices obtained by integrating shape function kernel products over all boundary elements of the pile;  $\mathbf{u}^{(p)}$  and  $\mathbf{t}^{(p)}$  are the generalized displacement and traction vectors of the nodes of the boundary elements of the pile. Dividing  $\mathbf{u}^{(p)}$  and  $\mathbf{t}^{(p)}$  into two parts corresponding to  $\Gamma_1$  and  $\Gamma_2$ , respectively, and partitioning the coefficient matrices  $\mathbf{G}^{(p)}$  and  $\mathbf{H}^{(p)}$  accordingly, equation (6) is rewritten as follows

$$\begin{bmatrix} \mathbf{H}_1^{(p)} & \mathbf{H}_2^{(p)} \end{bmatrix} \begin{Bmatrix} \mathbf{u}_1^{(p)} \\ \mathbf{u}_2^{(p)} \end{Bmatrix} = \begin{bmatrix} \mathbf{G}_1^{(p)} & \mathbf{G}_2^{(p)} \end{bmatrix} \begin{Bmatrix} \mathbf{t}_1^{(p)} \\ \mathbf{t}_2^{(p)} \end{Bmatrix} \quad (7)$$

in which the subscripts 1 and 2 represent the boundaries  $\Gamma_1$  and  $\Gamma_2$  of the pile, respectively;  $\mathbf{u}_j^{(p)}, \mathbf{t}_j^{(p)}, j=1, 2$  denote the generalized displacement and traction vectors for the boundaries  $\Gamma_j, j=1, 2$  of the pile, respectively;  $\mathbf{H}_1^{(p)}, \mathbf{H}_2^{(p)}$  and  $\mathbf{G}_1^{(p)}, \mathbf{G}_2^{(p)}$  are the sub-matrices of the coefficient matrices  $\mathbf{H}^{(p)}$  and  $\mathbf{G}^{(p)}$  of the pile, corresponding to the boundaries  $\Gamma_1$  and  $\Gamma_2$ , respectively.

Likewise, applying equation (5) to the boundary integral equation of the half-space soil and implementing the similar BEM procedure, the boundary element formulation for the half-space soil is derived as follows

$$\mathbf{H}^{(s)} \mathbf{u}^{(s)} = \mathbf{G}^{(s)} \mathbf{t}^{(s)} \quad (8)$$

in which the superscript  $s$  denotes the half-space soil;  $\mathbf{u}^{(s)}$  and  $\mathbf{t}^{(s)}$  are the generalized displacement and traction vectors of the nodes of the boundary elements of the half-space soil;  $\mathbf{G}^{(s)}$  and  $\mathbf{H}^{(s)}$  are the coefficient matrices. Analogously, partitioning the coefficient matrices as well as the displacement and traction vectors in equation (8) corresponding to the boundaries  $\Gamma_1$  and  $\Gamma_3$  of the half-space soil, the boundary element formulation (8) for the half-space soil is reformulated as follows

$$\begin{bmatrix} \mathbf{H}_1^{(s)} & \mathbf{H}_3^{(s)} \end{bmatrix} \begin{Bmatrix} \mathbf{u}_1^{(s)} \\ \mathbf{u}_3^{(s)} \end{Bmatrix} = \begin{bmatrix} \mathbf{G}_1^{(s)} & \mathbf{G}_3^{(s)} \end{bmatrix} \begin{Bmatrix} \mathbf{t}_1^{(s)} \\ \mathbf{t}_3^{(s)} \end{Bmatrix} \quad (9)$$

in which  $\mathbf{u}_j^{(s)}, \mathbf{t}_j^{(s)}, j=1, 3$  denote the generalized displacement and traction vectors for the boundaries  $\Gamma_j, j=1, 3$  of the half-space soil, respectively,  $\mathbf{H}_1^{(s)}, \mathbf{H}_3^{(s)}$  and  $\mathbf{G}_1^{(s)}, \mathbf{G}_3^{(s)}$  are the sub-matrices of the coefficient matrices of the half-space soil associated with the boundaries  $\Gamma_1$  and  $\Gamma_3$  of the half-space soil, respectively.

At the interface  $\Gamma_1$ , the pile and soil should satisfy displacement and traction continuity conditions. The boundary conditions at the top of the pile ( $\Gamma_2$ ) are determined by the loads applied at the top of the pile. Thus,  $\mathbf{t}_2^{(p)}$  in equation (7) is assumed to be known *a priori*. Moreover, at the surface  $\Gamma_3$ , the half-space soil is supposed to be stress free. As a result, the following continuity conditions and boundary condition should be fulfilled along the interface  $\Gamma_1$  and the boundary  $\Gamma_3$ , respectively

$$\mathbf{u}_1^{(p)} = \mathbf{u}_1^{(s)}, \quad \mathbf{t}_1^{(p)} = -\mathbf{t}_1^{(s)}, \quad \mathbf{t}_3^{(s)} = \mathbf{0} \quad (10)$$

By using the boundary element formulations for the pile and soil as given by equations (7) and (9) as well as the continuity conditions and boundary condition as shown in equation (10), a coupled BEM model for the pile-soil system is obtained as follows

$$\begin{bmatrix} \mathbf{H}_1^{(p)} - \mathbf{G}_1^{(p)} & \mathbf{H}_2^{(p)} & \mathbf{0} \\ \mathbf{H}_1^{(s)} & \mathbf{G}_1^{(s)} & \mathbf{0} & \mathbf{H}_3^{(s)} \end{bmatrix} \begin{bmatrix} \mathbf{u}_1^{(p)} & \mathbf{t}_1^{(p)} & \mathbf{u}_2^{(p)} & \mathbf{u}_3^{(s)} \end{bmatrix}^T = \begin{bmatrix} \mathbf{G}_2^{(p)} \mathbf{t}_2^{(p)} \\ \mathbf{0} \end{bmatrix} \quad (11)$$

#### IV. ANALYSIS OF THE SUPER STRUCTURE OF THE DPV IN THE WAVENUMBER DOMAIN

In this section, the governing equations for the piers and beams of the viaduct undergoing in-plane and out-of-plane vibrations will be outlined. As noted above, when subjected to

seismic waves, both in-plane and out-of-plane vibrations will occur in the periodic viaduct. The in-plane vibration of the periodic viaduct will involve the longitudinal and in-plane flexural vibrations of the piers and beams, while the out-of-plane vibration of the periodic viaduct consists of the torsional and out-of-plane flexural vibrations of the piers and beams.

A. The Transfer Matrices for the Piers and Beams

As the piers are treated as 1-D rods and beams, their transfer matrices can be derived by the conventional vibration theories for a rod and beam undergoing axial and flexural vibrations, respectively. For simplicity, the vibration of the beams in this study is described by the Bernoulli-Euler beam theory [17]. Thus, the frequency-wavenumber domain equations of motion for the longitudinal and in-plane flexural vibrations of the pier in the n-th span of the periodic viaduct are given as follows [17]

$$E_d \frac{d^2 u_d^{(n)}(z^{(e)})}{dz^{(e)2}} + \rho_d \omega^2 u_d^{(n)}(z^{(e)}) = 0,$$

$$E_d I_{dl} \frac{d^4 v_d^{(n)}(z^{(e)})}{dz^{(e)4}} - \rho_d A_d \omega^2 v_d^{(n)}(z^{(e)}) = 0 \tag{12}$$

where the subscript d denotes the pier,  $\rho_d$  and  $E_d$  are the density and elastic modulus of the pier,  $A_d$  and  $I_{dl}$  are the cross section area and second moment of the cross section of the pier,  $u_d^{(n)}, v_d^{(n)}$  are the axial and transverse displacements, respectively,  $z^{(e)}$  denotes the local vertical coordinate of the cross-section of the pier.

For the sign convention of the internal forces of the pier, the following relations hold [17]

$$N_d^{(n)}(z^{(e)}) = E_d A_d \frac{du_d^{(n)}(z^{(e)})}{dz^{(e)}},$$

$$M_{dl}^{(n)}(z^{(e)}) = -E_d I_{dl} v_d^{(n)''}(z^{(e)}),$$

$$Q_{dl}^{(n)}(z^{(e)}) = -\frac{dM_{dl}^{(n)}(z^{(e)})}{dz^{(e)}} \tag{13}$$

where  $N_d^{(n)}, Q_{dl}^{(n)}, M_{dl}^{(n)}$  are the axial, shear force and moment of the cross-section. For the pier of the n-th span undergoing in-plane vibration, the displacement, internal force vectors and state vector for an arbitrary cross-section are defined as follows

$$\mathbf{q}_{dl}^{(n)}(z^{(e)}) = \{u_d^{(n)}(z^{(e)}), v_d^{(n)}(z^{(e)}), \theta_{dl}^{(n)}(z^{(e)})\}^T,$$

$$\mathbf{f}_{dl}^{(n)}(z^{(e)}) = \{N_d^{(n)}(z^{(e)}), Q_{dl}^{(n)}(z^{(e)}), M_{dl}^{(n)}(z^{(e)})\}^T,$$

$$\Psi_{dl}^{(n)}(z^{(e)}) = \{\mathbf{q}_{dl}^{(n)T}(z^{(e)}), \mathbf{f}_{dl}^{(n)T}(z^{(e)})\}^T \tag{14}$$

in which  $\theta_{dl}^{(n)}$  is the rotation angle of the cross-section

$z^{(e)}$  of the n-th pier,  $\mathbf{q}_{dl}^{(n)}, \mathbf{f}_{dl}^{(n)}$  and  $\Psi_{dl}^{(n)}$  represent the displacement and internal force vectors as well as the state vector, respectively. By using equations (12), (13) and (14), the transfer matrix for the pier undergoing in-plane vibration can be derived.

Likewise, the frequency-wavenumber domain equations of motion for the longitudinal and in-plane flexural vibrations of the beams of the n-th span have the following expressions

$$E_b \frac{d^2 u_b^{(n)}(x^{(e)})}{dx^{(e)2}} + \rho_b \omega^2 u_b^{(n)}(x^{(e)}) = 0,$$

$$E_b I_{bl} \frac{d^4 v_b^{(n)}(x^{(e)})}{dx^{(e)4}} - \rho_b A_b \omega^2 v_b^{(n)}(x^{(e)}) = 0 \tag{15}$$

where the subscript b denotes the beams,  $\rho_b$  and  $E_b$  are the density and elastic modulus of the beams,  $A_b$  and  $I_{bl}$  are the cross section area and second moment of the cross section of the beams,  $u_b^{(n)}, v_b^{(n)}$  are the axial and transverse displacements, respectively,  $x^{(e)}$  represents the local longitudinal coordinate for the cross-section of the beams.

For the internal forces of the beams, the following relations hold

$$N_b^{(n)}(x^{(e)}) = E_b A_b \frac{du_b^{(n)}(x^{(e)})}{dx^{(e)}},$$

$$M_{bl}^{(n)}(x^{(e)}) = -E_b I_{bl} v_b^{(n)''}(x^{(e)}),$$

$$Q_{bl}^{(n)}(x^{(e)}) = \frac{dM_{bl}^{(n)}(x^{(e)})}{dx^{(e)}} \tag{16}$$

where  $N_b^{(n)}, Q_{bl}^{(n)}, M_{bl}^{(n)}$  are the axial and shear forces and moment of the cross-section. For the beams of the n-th span undergoing in-plane vibration, the displacement and internal force vectors and the state vector at a cross-section  $x^{(e)}$  are defined as follows

$$\mathbf{q}_{bl}^{(n)}(x^{(e)}) = \{u_b^{(n)}(x^{(e)}), v_b^{(n)}(x^{(e)}), \theta_{bl}^{(n)}(x^{(e)})\}^T,$$

$$\mathbf{f}_{bl}^{(n)}(x^{(e)}) = \{N_b^{(n)}(x^{(e)}), Q_{bl}^{(n)}(x^{(e)}), M_{bl}^{(n)}(x^{(e)})\}^T,$$

$$\Psi_{bl}^{(n)}(x^{(e)}) = \{\mathbf{q}_{bl}^{(n)T}(x^{(e)}), \mathbf{f}_{bl}^{(n)T}(x^{(e)})\}^T \tag{17}$$

in which  $\theta_{bl}^{(n)}$  is the rotation angle of the cross-section  $x^{(e)}$  of the beams,  $\mathbf{q}_{bl}^{(n)}, \mathbf{f}_{bl}^{(n)}$  and  $\Psi_{bl}^{(n)}$  represent the displacement and internal force vectors as well as the state vector for the cross-section of the beams, respectively. By using equations (15), (16) and (17), the transfer matrix for the beams undergoing in-plane vibration can be derived, which is similar to that for the pier and thus is omitted in this study.

As mentioned previously, the out-of-plane vibration of the periodic viaduct involves the torsional and out-of-plane flexural vibrations of the beams and piers. The frequency-wavenumber domain equations of motion for the

torsional and out-of-plane flexural vibrations of the n-th pier are as follows [17]

$$\mu_d \frac{d^2 \phi_d^{(n)}(z^{(e)})}{dz^{(e)2}} + \rho_d \omega^2 \tilde{\phi}_d^{(n)}(z^{(e)}) = 0,$$

$$E_d I_{do} \frac{d^4 w_d^{(n)}(z^{(e)})}{dz^{(e)4}} - \rho_d A_d \omega^2 w_d^{(n)}(z^{(e)}) = 0 \quad (18)$$

where  $\mu_d$  is the shear modulus of the pier,  $I_{do}$  is the second moment of the cross section of the pier for the out-of-plane vibration,  $\phi_d^{(n)}$  and  $w_d^{(n)}$  are the twist angle and deflection of the pier, respectively.

For the sign convention for the internal forces, the following relations hold [17]

$$m_d^{(n)}(z^{(e)}) = \mu_d I_{dp} \frac{d\phi_d^{(n)}(z^{(e)})}{dz^{(e)}},$$

$$M_{do}^{(n)}(z^{(e)}) = -E_d I_{do} w_d^{(n)'}(z^{(e)}),$$

$$Q_{do}^{(n)}(z^{(e)}) = -\frac{dM_{do}^{(n)}(z^{(e)})}{dz^{(e)}} \quad (19)$$

where  $I_{dp}$  is the polar moment of inertia of the cross section of the pier,  $m_d^{(n)}$ ,  $Q_{do}^{(n)}$ ,  $M_{do}^{(n)}$  are the torque, shear force and bending moment of the cross-section of the pier. For the pier undergoing out-of-plane vibration, the displacement and internal force vectors as well as the state vector at an arbitrary cross-section are defined as follows

$$\mathbf{q}_{do}^{(n)}(z^{(e)}) = \{\phi_d^{(n)}(z^{(e)}), v_d^{(n)}(z^{(e)}), \theta_{do}^{(n)}(z^{(e)})\}^T,$$

$$\mathbf{f}_{do}^{(n)}(z^{(e)}) = \{m_d^{(n)}(z^{(e)}), Q_{do}^{(n)}(z^{(e)}), M_{do}^{(n)}(z^{(e)})\}^T,$$

$$\Psi_{do}^{(n)}(z^{(e)}) = \{\mathbf{q}_{do}^{(n)T}(z^{(e)}), \mathbf{f}_{do}^{(n)T}(z^{(e)})\}^T \quad (20)$$

where  $\theta_{do}^{(n)}$  is the rotation angle of the cross-section  $z^{(e)}$  of the pier,  $\mathbf{q}_{do}^{(n)}$ ,  $\mathbf{f}_{do}^{(n)}$  and  $\Psi_{do}^{(n)}$  represent the displacement and internal force vectors as well as the state vector for the cross-section of the pier, respectively. By using equations(18), (19) and (20), the transfer matrix for the pier undergoing out-of-plane vibration can be derived.

Analogously, the frequency-wavenumber domain equations of motion for the torsional and out-of-plane flexural vibrations of the beams of the n-th span have the following forms

$$\mu_b \frac{d^2 \phi_b^{(n)}(x^{(e)})}{dx^{(e)2}} + \rho_b \omega^2 \tilde{\phi}_b^{(n)}(x^{(e)}) = 0,$$

$$E_b I_{bo} \frac{d^4 w_b^{(n)}(x^{(e)})}{dx^{(e)4}} - \rho_b A_b \omega^2 w_b^{(n)}(x^{(e)}) = 0 \quad (21)$$

where  $\mu_b$ ,  $I_{bo}$  are the shear modulus and the second

moment of the cross section of the beams for the out-of-plane vibration, respectively,  $\phi_b^{(n)}$  and  $w_b^{(n)}$  are the twist angle and deflection of the beams, respectively.

For the internal forces of the beams, the following relations hold

$$m_b^{(n)}(x^{(e)}) = \mu_b I_{bp} \frac{d\phi_b^{(n)}(x^{(e)})}{dx^{(e)}},$$

$$M_{bo}^{(n)}(x^{(e)}) = -E_b I_{bo} w_b^{(n)'}(x^{(e)}),$$

$$Q_{bo}^{(n)}(x^{(e)}) = \frac{dM_{bo}^{(n)}(x^{(e)})}{dx^{(e)}} \quad (22)$$

where  $I_{bp}$  is the polar moment of inertia of the cross-section of the beams,  $m_b^{(n)}$ ,  $Q_{bo}^{(n)}$ ,  $M_{bo}^{(n)}$  are the torque, shear force and bending moment of the cross-section. For the beams undergoing out-of-plane vibration, the displacement and internal force vectors as well as the state vector at an arbitrary cross-section are as follows

$$\mathbf{q}_{bo}^{(n)}(x^{(e)}) = \{\phi_b^{(n)}(x^{(e)}), w_b^{(n)}(x^{(e)}), \theta_{bo}^{(n)}(x^{(e)})\}^T,$$

$$\mathbf{f}_{bo}^{(n)}(x^{(e)}) = \{m_b^{(n)}(x^{(e)}), Q_{bo}^{(n)}(x^{(e)}), M_{bo}^{(n)}(x^{(e)})\}^T,$$

$$\Psi_{bo}^{(n)}(x^{(e)}) = \{\mathbf{q}_{bo}^{(n)T}(x^{(e)}), \mathbf{f}_{bo}^{(n)T}(x^{(e)})\}^T \quad (23)$$

where  $\theta_{bo}^{(n)}$  is the rotation angle of the cross-section  $x^{(e)}$  of the beams,  $\mathbf{q}_{bo}^{(n)}$ ,  $\mathbf{f}_{bo}^{(n)}$  and  $\Psi_{bo}^{(n)}$  represent the displacement and internal force vectors as well as the state vector for the cross-section of the beams, respectively. By using equations(21), (22) and(23), the transfer matrix for the beams undergoing out-of-plane vibration can be derived, which is similar to that for the pier undergoing out-of-plane vibration and hence is omitted here.

### B. Coupling between the Pile-Soil System and the Super Structure

The displacement and force vectors of the n-th pile top are related to each other by the compliances of the pile, namely

$$\mathbf{q}_{pa}^{(n)}(0) = \mathbf{C}_{pa} \mathbf{f}_{pa}^{(n)}(0), \quad \alpha = I, O \quad (24)$$

where  $\mathbf{C}_p$  is the 3×3 compliance matrix for the pile, which can be obtained using the aforementioned BEM model for the pile-soil system.

As noted above, it is assumed that the pile and pier are rigidly connected, the displacement and force vectors of the bottom of the n-th pier are equal to those of the n-th pile top, namely

$$\mathbf{q}_{da}^{(n)}(L_d) = \mathbf{q}_{pa}^{(n)}(0), \quad \mathbf{f}_{da}^{(n)}(L_d) = \mathbf{f}_{pa}^{(n)}(0), \quad \alpha = I, O \quad (25)$$

By using equation (24) and (25), one has the following relation for the displacement and force vectors at the bottom of the n-th pier

$$\mathbf{q}_{da}^{(n)}(L_d) = \mathbf{C}_{pa} \mathbf{f}_{da}^{(n)}(L_d), \quad \alpha = I, O \quad (26)$$

Then, the relation between the state vectors at the top and bottom of the n-th pier is obtained as follows

$$\begin{Bmatrix} \mathbf{C}_{pa} \mathbf{f}_{da}^{(n)}(L_d) \\ \mathbf{f}_{da}^{(n)}(L_d) \end{Bmatrix} = \begin{bmatrix} \mathbf{T}_{\alpha qq}^{(d)}(L_d) & \mathbf{T}_{\alpha qf}^{(d)}(L_d) \\ \mathbf{T}_{\alpha fq}^{(d)}(L_d) & \mathbf{T}_{\alpha ff}^{(d)}(L_d) \end{bmatrix} \begin{Bmatrix} \mathbf{q}_{da}^{(n)}(0_+) \\ \mathbf{f}_{da}^{(n)}(0_+) \end{Bmatrix} \quad (27)$$

Using equation (27), the relation between the displacement and force vectors at the top of the n-th pier is obtained as follows

$$\begin{aligned} \mathbf{q}_{da}^{(n)}(0) &= \mathbf{C}_{da}(\boldsymbol{\kappa}) \mathbf{f}_{da}^{(n)}(0), \\ \mathbf{C}_{da} &= [\mathbf{T}_{\alpha qq}^{(d)}(L_d) - \mathbf{C}_{pa} \mathbf{T}_{\alpha fq}^{(d)}(L_d)]^{-1} [\mathbf{C}_{pa} \mathbf{T}_{\alpha ff}^{(d)}(L_d) - \mathbf{T}_{\alpha qf}^{(d)}(L_d)], \\ \alpha &= I, O \end{aligned} \quad (28)$$

By using the equilibrium conditions at the junction [21], the relation between the state vectors of the beam sections to the right and left of the n-th junction is obtained as follows

$$\begin{aligned} \begin{Bmatrix} \mathbf{q}_{ba}^{(n)}(0_+) \\ \mathbf{f}_{ba}^{(n)}(0_+) \end{Bmatrix} &= \mathbf{S}_{J\alpha} \begin{Bmatrix} \mathbf{q}_{ba}^{(n)}(0_-) \\ \mathbf{f}_{ba}^{(n)}(0_-) \end{Bmatrix}, \quad \mathbf{S}_{J\alpha} = \mathbf{A}_\alpha^{-1} \mathbf{B}_\alpha, \quad \alpha = I, O, \\ \mathbf{A}_\alpha &= \begin{bmatrix} \mathbf{J}_{lr\alpha} & \mathbf{J}_{ld\alpha} \mathbf{E}_{r\alpha}^{(b)} \\ \mathbf{J}_{mr\alpha} & \mathbf{J}_{md\alpha} \mathbf{E}_{r\alpha}^{(b)} - \mathbf{I}_{3 \times 3} \end{bmatrix}, \quad \mathbf{B}_\alpha = \begin{bmatrix} -\mathbf{J}_{ll\alpha} & \mathbf{I}_{3 \times 3} - \mathbf{J}_{ld\alpha} \mathbf{E}_{l\alpha}^{(b)} \\ -\mathbf{J}_{rl\alpha} & -\mathbf{J}_{rd\alpha} \mathbf{E}_{l\alpha}^{(b)} \end{bmatrix}, \\ \mathbf{E}_{l\alpha}^{(b)} &= \mathbf{C}_{d\alpha} \mathbf{E}_{l\alpha}^{(a)}, \quad \mathbf{E}_{r\alpha}^{(b)} = \mathbf{C}_{d\alpha} \mathbf{E}_{r\alpha}^{(a)} \end{aligned} \quad (29)$$

in which the matrix  $\mathbf{S}_{J\alpha}$  is referred to as the junction transfer matrix at the n-th BBP junction, and  $\mathbf{E}_{l\alpha}^{(a)}, \mathbf{E}_{r\alpha}^{(a)}$ ,

$\mathbf{J}_{ll\alpha}, \mathbf{J}_{lr\alpha}, \mathbf{J}_{ld\alpha}, \mathbf{J}_{rl\alpha}, \mathbf{J}_{rr\alpha}$  and  $\mathbf{J}_{rd\alpha}$  ( $\alpha = I, O$ ) are given in Appendix B. It is noted that for a periodic viaduct, the junction transfer matrix is identical for all the BBP junctions. By using equation (29) and the transfer matrices for the beams of the n-th span, one has the following relation for the state vectors at the right and left ends of the n-th span

$$\boldsymbol{\Psi}_{ba}^{(n)}\left(\frac{L}{2}\right) = \mathbf{T}_\alpha^{(b)}\left(\frac{L}{2}\right) \mathbf{S}_{J\alpha} \mathbf{T}_\alpha^{(b)}\left(\frac{L}{2}\right) \boldsymbol{\Psi}_{ba}^{(n)}\left(-\frac{L}{2}\right), \quad \alpha = I, O \quad (30)$$

where  $\mathbf{T}_\alpha^{(b)}(L/2)$  is the transfer matrix for the left and right beams,  $\boldsymbol{\Psi}_{ba}^{(n)}(-L/2)$  and  $\boldsymbol{\Psi}_{ba}^{(n)}(L/2)$  are the state vectors for the left and right ends of the n-th span, respectively.

### V. THE EIGHEVALUE EQUATION FOR THE SUPER-CELL OF THE DPV

A periodic structure with defects usually displays characteristics associated with defect state [1, 22]. Furthermore, the defect state characteristics of a periodic structure are usually relevant to its dynamic response. Consequently, to fully understand the dynamic response of a defected viaduct, it is necessary to investigate the relation between the response of the defected viaduct and its defect state. In this section, by means of the super-cell method and transfer matrix method, the eigenvalue equation for a super-cell of the defected viaduct will be derived, whereby the defect state of the defected viaduct can be identified.

Equation (30) implies that the transfer matrix for a standard span of the DPV has the following expression

$$\mathbf{T}_\alpha^{(q)} = \mathbf{T}_{\alpha R}^{(b_0)} \mathbf{S}_{J\alpha}^{(0)} \mathbf{T}_{\alpha L}^{(b_0)}, \quad \alpha = I, O \quad (31)$$

where the superscript  $q$  denotes the defected span of the viaduct.

Suppose that the super-cell contains  $2N + 1$  spans of the viaduct, the central span (the 0<sup>th</sup> span) being the defected span. By using the transfer matrices for the standard and defected spans, the relation between the state vectors at the right and left ends of the super-cell is obtained as follows

$$\begin{aligned} \boldsymbol{\Psi}_{ba}^{(n)}\left(\frac{L}{2}\right) &= \overbrace{\mathbf{T}_\alpha^{(s)} \cdots \mathbf{T}_\alpha^{(s)}}^N \mathbf{T}_\alpha^{(q)} \overbrace{\mathbf{T}_\alpha^{(s)} \cdots \mathbf{T}_\alpha^{(s)}}^N \boldsymbol{\Psi}_{ba}^{(n)}\left(-\frac{L}{2}\right), \\ \alpha &= I, O \end{aligned} \quad (32)$$

Using the Bloch theorem [23] and equation(32), the following eigenvalue equation is derived for the super-cell of the viaduct

$$\begin{aligned} \left[ \overbrace{\mathbf{T}_\alpha^{(s)} \cdots \mathbf{T}_\alpha^{(s)}}^N \mathbf{T}_\alpha^{(q)} \overbrace{\mathbf{T}_\alpha^{(s)} \cdots \mathbf{T}_\alpha^{(s)}}^N - e^{-i \kappa_s L_s} \mathbf{I}_{6 \times 6} \right] \boldsymbol{\Psi}_{ba}^{(n)}\left(-\frac{L}{2}\right) &= \mathbf{0}, \\ L_s &= 2NL + L_q, \quad \alpha = I, O \end{aligned} \quad (33)$$

in which  $\kappa_s$  denotes the wavenumbers for the characteristic waves of the super-cell;  $L_q$  and  $L_s$  are the lengths of the defected span and super-cell, respectively. Solution of equation (33) yields the energy bands of the super-cell, by which the defect state of the super-cell of the DPV can be identified.

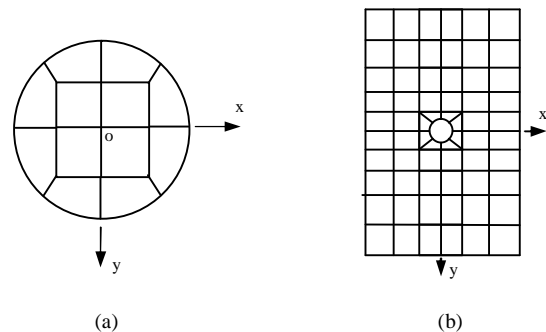


Fig. 3 The discretization schemes for the top and bottom of the piles as well as that for the surface of the half-space soil: (a) the discretization scheme for the piles; (b) the discretization scheme for the soil

### VI. NUMERICAL RESULTS AND CORRESPONDING ANALYSIS

In this section, based on the proposed model, some numerical results will be presented, which include the Influence of different defects on on the energy bands for the super cell of the DPV undergoing In-plane vibration and out-of-plane vibration.

In the numerical examples, the cross-sections of the piles and piers of the viaduct are assumed to be circular, while those of the beams are rectangular. The parameters for the pier,

beams and the stiffnesses of the linking springs of the standard span and those for the half-space soil are given by Table 1 and 2, respectively.

Table 1 The geometrical and material parameters of the soil, piles, piers and beams

The length of each span of the periodic viaduct ( $L$ )	20.0 m
The length and radius of the piles ( $L_p, R_p$ )	15.0 m, 1.0 m
The height and radius of the piers ( $L_d, R_d$ )	10.0 m, 1.0 m
The width and depth of the rectangular cross-section of the beams ( $w_b, h_b$ )	3.0 m, 1.0 m
The shear modulus, Poisson's ratio and density for the half-space soil ( $\mu_s, \nu_s, \rho_s$ )	$2.0 \times 10^7$ Pa, 0.4, $2.0 \times 10^3$ kg/m <sup>3</sup>
The Young's modulus, Poisson's ratio and density for the piles ( $E_p, \nu_p, \rho_p$ )	$2.8 \times 10^{10}$ Pa, 0.2, $2.4 \times 10^3$ kg/m <sup>3</sup>
The Young's modulus, Poisson's ratio and density for the piers ( $E_d, \nu_d, \rho_d$ )	$2.8 \times 10^{10}$ Pa, 0.2, $3.0 \times 10^3$ kg/m <sup>3</sup>
The Young's modulus, Poisson's ratio and density for the beams ( $E_b, \nu_b, \rho_b$ )	$2.8 \times 10^{10}$ Pa, 0.2, $3.6 \times 10^3$ kg/m <sup>3</sup>
The calculated frequency range of the incident Rayleigh wave ( $f$ )	0~50 Hz

The 2-D eight-node isoparametric boundary element [19] is used to discretize the boundaries of the pile and half-space soil. The top and bottom of the piles in both the standard span and defected span are discretized by twelve isoparametric boundary elements as shown in Figure 3 (a). The side boundary of the pile is divided into fifteen segments evenly, and each segment is discretized by eight elements evenly. To truncate the surface of the half-space soil, the surface of the half-space soil is covered by suitable numbers of vertical and horizontal boundary element layers (Figure 3(b)). The numbers of vertical and horizontal boundary element layers used to cover the soil surface for different frequency ranges are given in Table 3.

Table 2 The stiffness of the beam-beam, left beam-pier and right beam-pier springs

The stiffnesses of the beam-beam spring for the in-plane vibration ( $k_t^{(t)}, k_{II}^{(s)}, k_{II}^{(b)}$ )	$1.0 \times 10^8$ N/m, $1.0 \times 10^8$ N/m, $1.0 \times 10^7$ N.m/rad
The stiffnesses of the left beam-pier spring for the in-plane vibration ( $k_l^{(t)}, k_{II}^{(s)}, k_{II}^{(b)}$ )	$1.0 \times 10^8$ N/m, $1.0 \times 10^8$ N/m, $1.0 \times 10^7$ N.m/rad
The stiffnesses of the right beam-pier spring for the in-plane vibration ( $k_r^{(t)}, k_{rI}^{(s)}, k_{rI}^{(b)}$ )	$1.0 \times 10^8$ N/m, $1.0 \times 10^8$ N/m, $1.0 \times 10^7$ N.m/rad
The stiffnesses of the beam-beam spring for the out-of-plane vibration ( $k_t^{(r)}, k_{tO}^{(s)}, k_{tO}^{(b)}$ )	$1.0 \times 10^7$ N.m/rad, $1.0 \times 10^8$ N/m, $1.0 \times 10^8$ N.m/rad
The stiffnesses of the left beam-pier spring for the out-of-plane vibration ( $k_l^{(r)}, k_{lO}^{(s)}, k_{lO}^{(b)}$ )	$1.0 \times 10^8$ N.m/rad, $1.0 \times 10^8$ N/m, $1.0 \times 10^8$ N.m/rad
The stiffnesses of the right beam-pier spring for the out-of-plane vibration ( $k_r^{(r)}, k_{rO}^{(s)}, k_{rO}^{(b)}$ )	$1.0 \times 10^8$ N.m/rad, $1.0 \times 10^8$ N/m, $1.0 \times 10^8$ N.m/rad

Table 3 The numbers of the vertical and horizontal boundary element layers used to discretize the surface of the half-space soil for different frequency

ranges

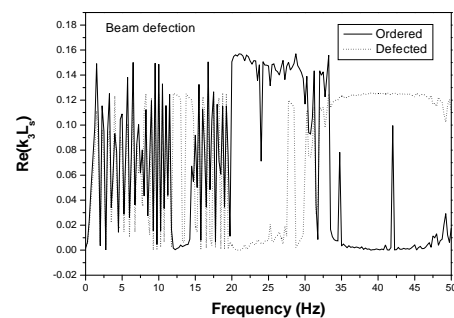
	BEM for a single pile (vertical $\times$ horizontal)
0-5Hz	18 $\times$ 18
5-20 Hz	16 $\times$ 16
20-40Hz	18 $\times$ 18
40-50 Hz	20 $\times$ 20

Table 4 The stiffness of the defected beam-beam, left beam-pier and right beam-pier springs

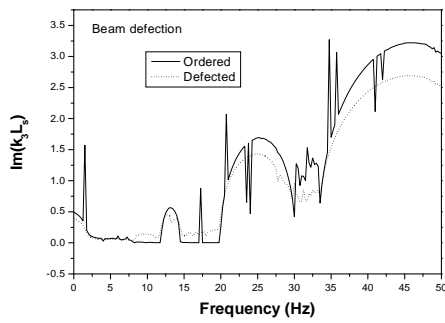
The stiffnesses of the beam-beam spring for the in-plane vibration ( $k_t^{(t)}, k_{II}^{(s)}, k_{II}^{(b)}$ )	$6.5 \times 10^8$ N/m, $6.5 \times 10^8$ N/m, $6.5 \times 10^7$ N.m/rad
The stiffnesses of the left beam-pier spring for the in-plane vibration ( $k_l^{(t)}, k_{II}^{(s)}, k_{II}^{(b)}$ )	$6.5 \times 10^8$ N/m, $6.5 \times 10^8$ N/m, $6.5 \times 10^7$ N.m/rad
The stiffnesses of the right beam-pier spring for the in-plane vibration ( $k_r^{(t)}, k_{rI}^{(s)}, k_{rI}^{(b)}$ )	$6.5 \times 10^8$ N/m, $6.5 \times 10^8$ N/m, $6.5 \times 10^7$ N.m/rad
The stiffnesses of the beam-beam spring for the out-of-plane vibration ( $k_t^{(r)}, k_{tO}^{(s)}, k_{tO}^{(b)}$ )	$6.5 \times 10^7$ N.m/rad, $6.5 \times 10^8$ N/m, $6.5 \times 10^8$ N.m/rad
The stiffnesses of the left beam-pier spring for the out-of-plane vibration ( $k_l^{(r)}, k_{lO}^{(s)}, k_{lO}^{(b)}$ )	$6.5 \times 10^8$ N.m/rad, $6.5 \times 10^8$ N/m, $6.5 \times 10^8$ N.m/rad
The stiffnesses of the right beam-pier spring for the out-of-plane vibration ( $k_r^{(r)}, k_{rO}^{(s)}, k_{rO}^{(b)}$ )	$6.5 \times 10^8$ N.m/rad, $6.5 \times 10^8$ N/m, $6.5 \times 10^8$ N.m/rad

A. Influence of Different Defects on the Energy Bands for the Super Cell of the DPV Undergoing In-plane Vibration

Figure 4, Figure 5 and Figure 6 plot the Influence of beam deflection (the length of the beams in the defected span is 12.5m), pier deflection (the height of the pier in the defected span is 15.0m) and spring deflection (the stiffnesses of the defected springs in the defected span are given in Table 4) in the BBP junction on on the energy bands for the characteristic waves ( $K_3L_S$ ) of the super-cells (consist of twenty-three spans) of the DPV undergoing in-plane vibration respectively. As the first and second characteristic waves are highly attenuative, only the energy bands for the third characteristic wave are presented.



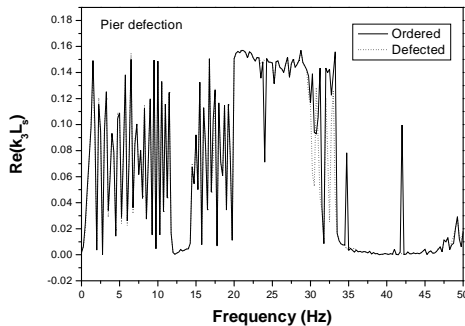
(a) the real part of the wavenumber



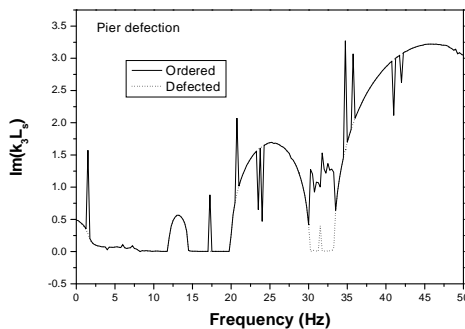
(b) the imaginary part of the wavenumber

Fig. 4 Influence of beam deflection on the energy bands of the third characteristic wave of the super-cells undergoing in-plane vibration

Figure 4 shows that in the calculated frequency range, several pass bands occur for both the OPV and DPV. But, compared with the ordered case, additional pass bands occur when the frequency exceeds 20.0Hz. This indicates that the defected span amplifies the dynamic response of the DPV and results in more resonances, which also can be seen from Figure 5 and Figure 6. Comparing these figures, we can see that, the influence of beam deflection on the energy bands for the super-cells is more apparent than pier deflection and spring deflection. However, when the defect lies in the piers, the imaginary part of the wavenumbers in the additional passbands are much lower, although it does not result in more passbands than the beam deflection and spring deflection do. This means the additional resonances it results in maybe more violent.

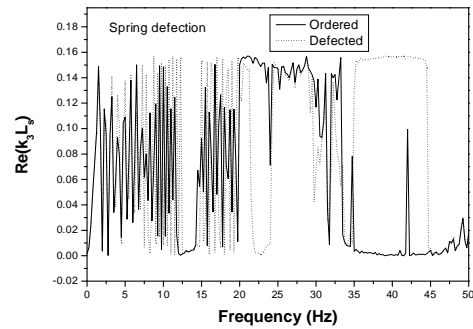


(a) the real part of the wavenumber

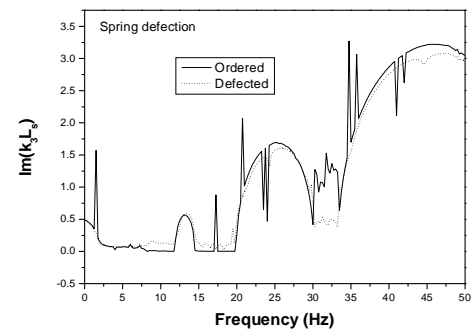


(b) the imaginary part of the wavenumber

Fig. 5 Influence of pier deflection on the energy bands of the third characteristic wave of the super-cells undergoing in-plane vibration



(a) the real part of the wavenumber

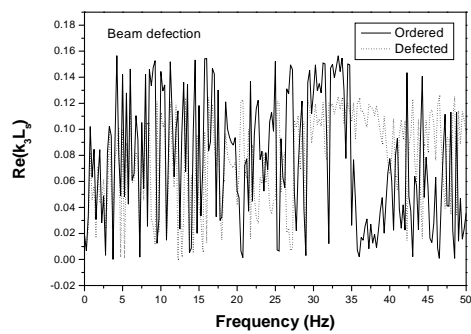


(b) the imaginary part of the wavenumber

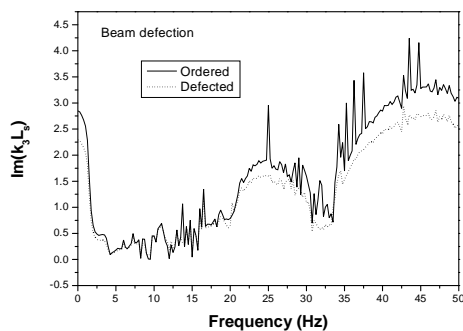
Fig. 6 Influence of spring deflection on the energy bands of the third characteristic wave of the super-cells undergoing in-plane vibration

**B. Influence of Different Defects on the Energy Bands for the Super Cell of the DPV Undergoing Out-of-Plane Vibration**

Figure 7, Figure 8 and Figure 9 plot the Influence of beam deflection (the length of the beams in the defected span is 12.5m), pier deflection (the height of the pier in the defected span is 15.0m) and spring deflection (the stiffnesses of the defected springs in the defected span are given in Table 4) in the BBP junction on on the energy bands for the characteristic waves ( $K_3L_3$ ) of the super-cells (consist of twenty-three spans) of the DPV undergoing out-of-plane vibration respectively.

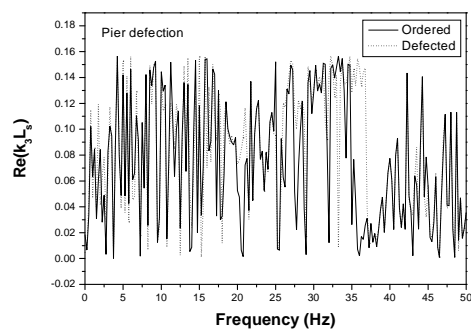


(a) the real part of the wavenumber

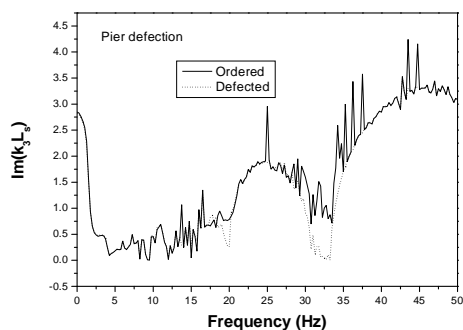


(b) the imaginary part of the wavenumber

Fig. 7 Influence of beam deflection on the energy bands of the third characteristic wave of the super-cells undergoing out-of-plane vibration

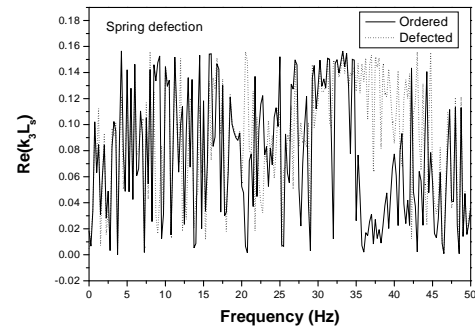


(a) the real part of the wavenumber

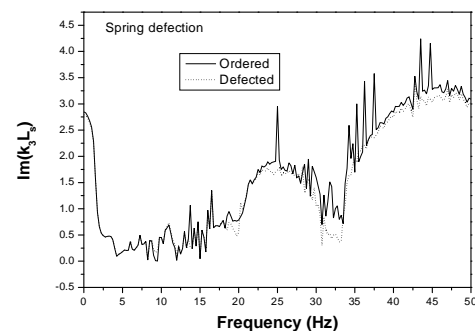


(b) the imaginary part of the wavenumber

Fig. 8 Influence of pier deflection on the energy bands of the third characteristic wave of the super-cells undergoing out-of-plane vibration



(a) the real part of the wavenumber



(b) the imaginary part of the wavenumber

Fig. 9 Influence of spring deflection on the energy bands of the third characteristic wave of the super-cells undergoing out-of-plane vibration

As in the in-plane vibration case, additional pass bands occur in the DPV, suggesting that the defected span amplifies the out-of-plane dynamic response of the DPV and results in more resonances too. Comparison of these three figures, we can also see that, the influence of beam deflection on the energy bands for the super-cells is more apparent than pier deflection and spring deflection, and pier deflection may result in more violent resonances.

## VII. CONCLUSION

A model for the analysis of the influence of different defects on the energy bands for the super cell of a DPV has been developed in this paper. Obviously, the proposed model is a useful tool for conducting aseismic design for various DPVs. For the inhomogeneous piers and beams, sub-division of piers and beams is a prerequisite for the establishment of the corresponding model. Alternatively, the finite element method can be used to discretize the inhomogeneous piers and beams and similar models can also be developed. Also, our model can be easily extended to account for the DPV with several defected spans.

Numerical results show that the defected span of the DPV has a pronounced influence on the dynamic response of the DPV. The defects amplify the dynamic response of the DPV

and results in more resonances, i.e., when the DPV is subjected to seismic waves, the dynamic responses of the spans near the defected span are amplified considerably. In summary, the presence of the defected span makes the DPV more vulnerable when exposed to seismic waves. As a result, for periodic viaducts with defects, it is important to mitigate the influence of the defected spans by choosing suitable geometrical and material parameters for the defected spans.

ACKNOWLEDGEMENT

Financial support received from the National Natural Science Foundation of China (No. 51078171) is highly acknowledged by the authors.

REFERENCES

[1] M.M. Sigalas. Defect states of acoustic waves in two-dimensional lattice of solid cylinders, J Appl Phys. vol. 84, pp. 3026–3030, 1998.  
 [2] C.H. Hodges. Confinement of vibration by structure irregularity, J Sound Vib. vol. 82, pp. 411–424, 1982.  
 [3] L. Brillouin. Wave propagation in periodic structures, Dover Public Inc, New York. 1946.  
 [4] D.J. Mead. Free wave propagation in periodically supported infinite beams, J Sound Vib. vol. 11, pp. 181–197, 1970.  
 [5] D.J. Mead. Wave propagation in continuous periodic structures: Research contributions from Southampton, J Sound Vib. vol. 190, pp. 495–524, 1996.  
 [6] D.J. Mead. A general theory of harmonic wave propagation in linear periodic systems with multiple coupling, J Sound Vib. vol. 27, pp. 235–260, 1973.  
 [7] Y.K. Lin. Free vibrations of a continuous beam on elastic supports, Int J Mech Sci. vol.4, pp. 409–423, 1962.  
 [8] F.G. Wu, Z.Y. Liu, Y.Y. Liu. Stop gaps and single defect states of acoustic waves in two-dimensional lattice of liquid cylinders, Chin Phys Lett. vol. 18, pp. 785–787, 2001.  
 [9] F.G. Wu. Point defect states in two-dimensional phononic crystals, Phys Lett. vol. 292, pp. 198–202, 2001.  
 [10] Y.K. Lin, J.N. Yang. Free vibration of a disordered periodic beam, J Appl Mech. vol. 41, pp. 383–391, 1974.  
 [11] J.N. Yang, Y.K. Lin. Frequency response function of a disordered periodic beam, J Sound Vib. vol. 38, pp. 317–340, 1975.  
 [12] D.J. Mead. Wave propagation and natural modes in periodic systems: Mono-coupled systems, J Sound Vib. vol. 40, pp. 1–18, 1975.  
 [13] D.J. Mead. Wave propagation and natural modes in periodic systems: Multi-coupled systems, with and without damping, J Sound Vib. vol. 40, pp. 19–39, 1975.  
 [14] D.J. Mead, A.S. Bansal. Mono-coupled periodic systems with a single disorder: Free wave propagation, J Sound Vib. vol. 61, pp. 481–496, 1978.  
 [15] A.S. Bansal. Free wave motion in periodic systems with multiple disorders, J Sound Vib. vol. 60, pp. 389–400, 1978.  
 [16] D.J. Mead, A.S. Bansal. Mono-coupled periodic systems with a single disorder: Response to convected loadings, J Sound Vib. vol. 61, pp. 497–515, 1978.  
 [17] K.F. Graff, Wave motion in elastic solids. Clarendon Press, Oxford, 1975.  
 [18] A.V. Oppenheim, A.S. Willsky, I.T. Young. Signals and systems, 2nd ed, Prentice Hall Englewood Cliffs, New Jersey, 1983.  
 [19] D. Clouteau, M.L. Elhabet, D. Aubry. Periodic BEM and FEM-BEM Coupling, COMPUT MECH. vol. 25, pp. 567–577, 2000.  
 [20] G.D. Manolis, D.E. Beskos. Boundary element methods in elastodynamics, Unwin Hyman, London, 1988.  
 [21] J.F. Lu, H.Y. Yuan. The sequence Fourier transform method for the analysis of a periodic viaduct subjected to non-uniform seismic. ACTA MECH, 2013.  
 [22] G. Beer, L. Smith, C. Duenser. The boundary element method with

programming: For engineers and scientists, Springer, Berlin, 2008.  
 [23] C. Kittel. Introduction to solid state physics, 7th ed, John Wiley & Sons, Inc, New York, 1996.

APPENDIX A-- THE FREQUENCY DOMAIN GREEN'S FUNCTION FOR A THREE-DIMENSIONAL ELASTIC MEDIUM

The frequency domain Green's functions  $U_{ij}$  and  $T_{ij}$  for an elastic medium have the following form

$$U_{ij} = \frac{1}{4\pi\mu} (\psi\delta_{ij} - \chi r_i r_j),$$

$$T_{ij} = \frac{1}{4\pi} \left[ A \left( \delta_{ij} \frac{\partial r}{\partial \mathbf{n}} + r_{,j} n_i \right) + B \left( n_j r_{,i} - 2r_{,i} r_{,j} \frac{\partial r}{\partial \mathbf{n}} \right) + C r_{,j} r_i \frac{\partial r}{\partial \mathbf{n}} + D r_{,i} n_j \right] \quad (A. 1)$$

and

$$\psi = \left( -\frac{C_2^2}{\omega^2 r^2} - i \frac{C_2}{\omega r} + 1 \right) \frac{e^{-i\omega r/C_2}}{r} + \frac{C_2^2}{C_1^2} \left( \frac{C_1^2}{\omega^2 r^2} + i \frac{C_1}{\omega r} \right) \frac{e^{-i\omega r/C_1}}{r},$$

$$\chi = \left( -\frac{3C_2^2}{\omega^2 r^2} - i \frac{3C_2}{\omega r} + 1 \right) \frac{e^{-i\omega r/C_2}}{r} + \frac{C_2^2}{C_1^2} \left( \frac{3C_1^2}{\omega^2 r^2} + i \frac{3C_1}{\omega r} - 1 \right) \frac{e^{-i\omega r/C_1}}{r} \quad (A. 2)$$

where  $A = d\psi/dr - \chi/r$ ,  $B = -2\chi/r$ ,  $C = -2d\chi/dr$ ,  $D = (C_1^2/C_2^2 - 2)(d\psi/dr - d\chi/dr - 2\chi/r)$ ,  $\mu$  is the shear modulus of the elastic medium, and  $C_1, C_2$  are the compressive and shear wave velocities of the elastic medium, respectively.

APPENDIX B—MATRICES IN EQUATION(29)

Matrices  $\mathbf{E}_{I\alpha}^{(a)}$  and  $\mathbf{E}_{r\alpha}^{(a)}$  ( $\alpha = I, O$ ) in equation(29) are given as follows

$$\mathbf{E}_{II}^{(a)} = \begin{bmatrix} 0 & 1 & 0 \\ -1 & 0 & 0 \\ 0 & 0 & -1 \end{bmatrix}, \quad \mathbf{E}_{rI}^{(a)} = \begin{bmatrix} 0 & -1 & 0 \\ 1 & 0 & 0 \\ 0 & 0 & 1 \end{bmatrix},$$

$$\mathbf{E}_{IO}^{(a)} = \begin{bmatrix} 0 & 0 & -1 \\ 0 & -1 & 0 \\ 1 & 0 & 0 \end{bmatrix}, \quad \mathbf{E}_{rO}^{(a)} = \begin{bmatrix} 0 & 0 & 1 \\ 0 & 1 & 0 \\ -1 & 0 & 0 \end{bmatrix} \quad (B.1)$$

Matrices  $\mathbf{J}_{II\alpha}, \mathbf{J}_{Ira}, \mathbf{J}_{Id\alpha}, \mathbf{J}_{rI\alpha}, \mathbf{J}_{rr\alpha}$  and  $\mathbf{J}_{rd\alpha}$  ( $\alpha = I, O$ ) in equation(29) are given as follows

$$\begin{aligned}
 \mathbf{J}_{ll} &= \begin{bmatrix} -(k_i^{(t)} + k_{ll}^{(s)}) & 0 & 0 \\ 0 & -(k_{ll}^{(s)} + k_l^{(t)}) & 0 \\ 0 & 0 & k_{ll}^{(b)} + k_{ll}^{(t)} \end{bmatrix}, \quad \mathbf{J}_{lr} = \begin{bmatrix} k_i^{(t)} & 0 & 0 \\ 0 & k_{ll}^{(s)} & 0 \\ 0 & 0 & -k_{ll}^{(b)} \end{bmatrix}, \\
 \mathbf{J}_{lr} &= \begin{bmatrix} 0 & k_{ll}^{(s)} & 0 \\ k_l^{(t)} & 0 & 0 \\ 0 & 0 & k_{ll}^{(b)} \end{bmatrix}, \quad \mathbf{J}_{ro} = \begin{bmatrix} -(k_i^{(r)} + k_{ro}^{(b)}) & 0 & 0 \\ 0 & -(k_{ro}^{(s)} + k_o^{(s)}) & 0 \\ 0 & 0 & k_{ro}^{(b)} + k_r^{(r)} \end{bmatrix}, \\
 \mathbf{J}_{ro} &= \begin{bmatrix} k_i^{(r)} & 0 & 0 \\ 0 & k_{ro}^{(s)} & 0 \\ 0 & 0 & -k_{ro}^{(b)} \end{bmatrix}, \quad \mathbf{J}_{ro} = \begin{bmatrix} 0 & 0 & -k_{ro}^{(b)} \\ 0 & k_{ro}^{(s)} & 0 \\ -k_i^{(r)} & 0 & 0 \end{bmatrix}, \\
 \mathbf{J}_{rl} &= \begin{bmatrix} -k_i^{(t)} & 0 & 0 \\ 0 & -k_{ll}^{(s)} & 0 \\ 0 & 0 & k_{ll}^{(b)} \end{bmatrix}, \quad \mathbf{J}_{rl} = \begin{bmatrix} k_i^{(t)} + k_{rl}^{(s)} & 0 & 0 \\ 0 & k_{ll}^{(s)} + k_r^{(t)} & 0 \\ 0 & 0 & -(k_{ll}^{(b)} + k_{rl}^{(b)}) \end{bmatrix}, \\
 \mathbf{J}_{rl} &= \begin{bmatrix} 0 & -k_{rl}^{(s)} & 0 \\ -k_r^{(t)} & 0 & 0 \\ 0 & 0 & -k_{rl}^{(b)} \end{bmatrix}, \quad \mathbf{J}_{ro} = \begin{bmatrix} -k_i^{(r)} & 0 & 0 \\ 0 & -k_{ro}^{(s)} & 0 \\ 0 & 0 & k_{ro}^{(b)} \end{bmatrix}, \\
 \mathbf{J}_{ro} &= \begin{bmatrix} k_i^{(r)} + k_{ro}^{(b)} & 0 & 0 \\ 0 & k_{ro}^{(s)} + k_{ro}^{(s)} & 0 \\ 0 & 0 & -(k_{ro}^{(b)} + k_r^{(r)}) \end{bmatrix}, \quad \mathbf{J}_{ro} = \begin{bmatrix} 0 & 0 & k_{ro}^{(b)} \\ 0 & -k_{ro}^{(s)} & 0 \\ k_r^{(r)} & 0 & 0 \end{bmatrix}
 \end{aligned} \tag{B.2}$$